

Wall-mediated self-diffusion in slit and cylindrical pores

Hyungjun Kim,^{1,*} Changho Kim,² Eok Kyun Lee,¹ Peter Talkner,³ and Peter Hänggi³

¹*Department of Chemistry and School of Molecular Science (BK21), Korea Advanced Institute of Science and Technology, Daejeon 305-701, Republic of Korea*

²*Department of Mathematical Sciences, Korea Advanced Institute of Science and Technology, Daejeon 305-701, Republic of Korea*

³*Institut für Physik, Universität Augsburg, D-86135 Augsburg, Germany*

(Received 11 January 2008; published 21 March 2008)

Analytical and numerical simulation studies are performed on the diffusion of simple fluids in both thin slits and long cylindrical pores. In the region of large Knudsen numbers, where the wall-particle collisions outnumber the intermolecular collisions, we obtain analytical results for the self-diffusion coefficients for both slit and cylindrical pore shapes. The results show anomalous behavior of the mean square displacement and the velocity autocorrelation for the case of slits, unlike the case of cylindrical pores which shows standard Fick's law. Molecular dynamics simulations confirm the analytical results. We further study the wall-mediated diffusion behavior conducted by a Smoluchowski thermal wall and compare with our analytical results obtained from the stochastic thermal wall model proposed by Mon and Percus.

DOI: [10.1103/PhysRevE.77.031202](https://doi.org/10.1103/PhysRevE.77.031202)

PACS number(s): 51.10.+y, 47.45.-n, 68.43.Jk

I. INTRODUCTION

Transport phenomena of fluids in confined spaces have been of long-standing interest. Owing to the development of nanoscience, a number of interesting diffusion behaviors in systems with strong geometric confinement have been recently observed and studied. These systems include biological [1] and artificial [2,3] channels, carbon nanotubes [4], templated porous materials [5,6], molecularly imprinted materials [7], nanoporous catalysts [8,9], and membrane fuel cells [10]. Thus a comprehensive understanding of diffusion processes in porous systems has become essential.

The establishment of the relationship of the parameters characterizing a fluid in a nanopore—pore shape, pore size, and adsorbate's density—with its diffusivity has been a challenge to theoreticians [11–26]. The classical study of diffusion in a pore dates back to Knudsen's seminal work [27]. In his work, the diffusivity of a hard-sphere fluid in a cylindrical pore was obtained analytically in the low density limit. In the Knudsen diffusion regime, the intermolecular collisions are neglected and the particles diffuse in a wall-mediated manner. Each molecule performs a series of free flights and changes its directions after collisions with the pore wall. The wall collisions supply the stochastic driving force which is necessary for a diffusive motion of the particles. Thus a system in the Knudsen regime can be regarded as an ensemble of noninteracting hard-sphere particles in a confined geometry.

Several theoretical studies have been following since then [28–31]. Recently, Bhatia and his co-workers have studied the transport of soft spheres adsorbed in slit and cylindrical nanopores at low density [11], and then extended their study to a higher density region by including a viscous term obtained from the Navier-Stokes equations [12–16].

Numerous theoretical studies on this subject have been focused on the idealized geometries known as slit and cylindrical pores. In the Knudsen diffusion regime, the characteristic features of a self-diffusion coefficient show distinctive differences depending on the geometry of the pore. While the self-diffusion coefficient in a cylindrical pore has been known to be a finite quantity [27,28,32], there is a good reason that the self-diffusivity in a slit pore shows divergent behavior [18]. In order to circumvent the divergence and obtain a finite valued diffusion coefficient, Arya *et al.* introduced a transverse cutoff velocity, which is physically a reasonable compromise when considering real pore systems with a large but finite Knudsen number [18].

Various thermal wall models which have stochastic character have been introduced to describe the collision of gas molecules with a wall having a roughness on a realistic atomic scale. Knudsen assumed all the gas-wall collisions to be diffusive, i.e., every particle that collides with the wall loses its momentum and becomes fully thermalized (Knudsen wall) [27,33,34]. Knudsen's treatment was subsequently generalized by Smoluchowski [32]. He proposed a more realistic thermal wall model by using Maxwell's slip boundary condition at a wall-fluid interface [35]. His thermal wall model is designed to consider the diffusion of the particle affected by both random thermal scattering and specular (reflective) scattering motion (Smoluchowski wall). Another wall model which is simple enough to be treated in an analytical manner, but still contains the essential feature of a stochastic thermal wall, has been proposed by Mon and Percus (MP wall) [36,37]. In this model, in each collision with the wall, the component of the momentum perpendicular to the wall is reversed, while its component parallel to the wall is either reversed with a prescribed probability or otherwise is preserved. In spite of the simplicity, this wall model has the virtues that the average kinetic energy is conserved and that it is able to reflect the tendency of specular motion of the scattered particle by adjusting the reversal probability [36,37].

In this work we utilize these features of the MP wall to analytically examine the diffusion process of the fluid par-

*Present address: Materials and Process Simulation Center, Beckman Institute (139-74), California Institute of Technology, Pasadena, CA 91125, USA.

ticles confined in a micropore in the low density limit for various shapes of micropores. We obtain the diffusion coefficient as well as the long time behavior of the velocity autocorrelation function (VACF) in analytical forms and compare them with results obtained from a molecular dynamics (MD) simulation study for both cylindrical and slit pores. Moreover, we find that the MP wall model is essentially equivalent to the Knudsen-Smoluchowski wall model by choosing an adequate reversal probability.

The present paper is organized as follows. In Sec. II, analytical results of the mean square displacement in the low density limit are derived for the MP wall model. In Sec. III, numerical simulation results are presented which confirm our analytical results. Further, the relationship between the MP wall and the Knudsen-Smoluchowski wall are discussed. Concluding remarks follow in the last section.

II. BEHAVIORS OF THE MEAN SQUARE DISPLACEMENTS IN LOW DENSITY REGIONS

A. Analytical result for the slit pore

We consider a hard-sphere particle moving in a slit pore confined by two parallel walls separated by a distance of length L . We choose the coordinate axis so that the walls are parallel to the xy plane and located at $z = \pm \frac{1}{2}L$, respectively. It suffices to consider a single gas particle because in the Knudsen regime the particles are independent of each other. The considered particle, having diameter σ and mass m , is initially positioned at $(0, 0, z_0)$ with initial velocity \mathbf{v}_0 . Because of the confinement, the z component of the particle's position satisfies

$$-\frac{1}{2}\hat{L} \leq z \leq \frac{1}{2}\hat{L}, \quad (1)$$

where $\hat{L} = L - \sigma$ is the effective pore width in which the center of the particle can move.

Let us assume that the wall-particle interaction follows the mechanism of the MP wall with a longitudinal momentum reversal probability q . Then the particle moves freely except for the moment when it collides with a wall. A particle hitting either wall with the velocity $\mathbf{v}_{\text{in}} = (v_x, v_y, v_z)$ has an outgoing velocity determined by

$$\mathbf{v}_{\text{out}} = \begin{cases} (v_x, v_y, -v_z) & \text{w.p. } p = 1 - q, \\ (-v_x, -v_y, -v_z) & \text{w.p. } q, \end{cases} \quad (2)$$

where w.p. is an abbreviation of "with probability." So the magnitude of the particle velocity equals the constant values $|\mathbf{v}_0|$ through the whole process.

In order to construct the complete analytical description of the motion of a particle in a slit pore with MP walls, we start with the observation that the motion projected on the xy plane lies on a straight line, which depends on the initial position and velocity. Moreover, the time of free flight between subsequent collisions is constant. We denote the displacement of the particle from its initial position and the velocity by $\Delta \mathbf{x}$ and \mathbf{v} , respectively. The only possible values of the velocity projected onto the xy plane are $\bar{\mathbf{v}} = \pm \bar{\mathbf{v}}_0$,

where the bar over any vector $\mathbf{a} = (a_x, a_y, a_z)$ denotes its projection onto the xy plane, i.e., $\bar{\mathbf{a}} = (a_x, a_y, 0)$. Thus the displacement $\Delta \bar{\mathbf{x}}$ is parallel to the direction of $\bar{\mathbf{v}}_0$. We can set this direction as the x direction for our convenience. Then, the two-dimensional vector $\Delta \bar{\mathbf{x}}$ can be replaced by a scalar variable Δx .

In this coordinate system adapted to the particle motion, \mathbf{v}_0 can be written as $(v_0^x, 0, v_0^z)$, where v_0^x is the magnitude of the initial velocity projected on the xy plane, i.e., $v_0^x = |\mathbf{v}_0|$, and v_0^z is the component of the initial velocity normal to the xy plane. From now on, we assume, without loss of generality, $v_0^z \geq 0$. The case where $v_0^z \leq 0$ is essentially the same due to symmetry. Then the speed of the particle projected on the xy plane and the sojourn time between subsequent collisions become

$$v = v_0^x, \quad (3)$$

$$\tau = \frac{\hat{L}}{v_0^z}, \quad (4)$$

respectively. The time when the particle first hits one of the walls is given by

$$\tau_0 = \frac{\hat{L}/2 - z_0}{v_0^z}. \quad (5)$$

Therefore the dynamics of the considered particle is reduced to a one-dimensional problem.

We denote the conditional probability density of a particle starting at z_0 with lateral velocity v and transversal velocity v_0^z to proceed a lateral distance Δx at time t by $\rho(\Delta x, t | \tau_0, \tau, v)$, where for the sake of convenience we have expressed the conditions v_0^z and z_0 by the dynamical parameters τ and τ_0 . By a convenient translation of time t and position Δx , the lateral condition z_0 can always be shifted to the value $z_0 = -\frac{1}{2}\hat{L}$, i.e., to $\tau_0 = \tau$. Denoting the conditional probability density at $z_0 = -\frac{1}{2}\hat{L}$ by $\tilde{\rho}(\Delta x, t | \tau, v) = \rho(\Delta x, t | \tau_0 = \tau, \tau, v)$, the following relation holds for $0 \leq \tau_0 \leq \tau$.

$$\rho(\Delta x, t | \tau_0, \tau, v) = \tilde{\rho}(\Delta x + v(\tau - \tau_0), t + (\tau - \tau_0) | \tau, v) \quad (6)$$

which reveals that $\tilde{\rho}(\Delta x, t | \tau, v)$ contains the same information as $\rho(\Delta x, t | \tau_0, \tau, v)$.

Once an analytical result of $\rho(\Delta x, t | \tau_0, \tau, v)$ is known, the second moment of Δx and the mean square displacement (MSD) of an ensemble of noninteracting hard-sphere particles can be obtained by taking the average with respect to the initial position z_0 and the initial velocity \mathbf{v}_0 . Instead of taking an average over z_0 , we perform the equivalent average over τ_0 . Assuming a uniform distribution of z_0 on the interval $-\frac{1}{2}\hat{L} \leq z_0 \leq \frac{1}{2}\hat{L}$, so is τ_0 on $0 \leq \tau_0 \leq \tau$. The second moment of the displacement, conditioned on the initial velocity \mathbf{v}_0 , is defined as

$$\langle \Delta \bar{\mathbf{x}}^2(t) | \mathbf{v}_0 \rangle = K(t | \tau, v), \quad (7)$$

where

$$K(t|\tau, v) = \frac{1}{\tau} \int_0^\tau d\tau_0 \int_{-\infty}^\infty d(\Delta x) \rho(\Delta x, t|\tau_0, \tau, v) (\Delta x)^2. \quad (8)$$

For Maxwell-Boltzmann distributed initial velocities, the MSD becomes

$$\langle \Delta \bar{x}^2(t) \rangle = \int_0^\infty dv_0^x \int_{-\infty}^\infty dv_0^z K(t|\tau, v) \psi(v_0^x, v_0^z), \quad (9)$$

where

$$\psi(v_0^x, v_0^z) = \sqrt{\frac{m^3}{2\pi(k_B T)^3}} v_0^x \exp\left(-\frac{m\{(v_0^x)^2 + (v_0^z)^2\}}{2k_B T}\right). \quad (10)$$

An analytical derivation of $\tilde{\rho}(\Delta x, t|\tau, v)$ is feasible because the wall mediated diffusion problem is essentially determined by a discrete time persistent random walk on a one-dimensional lattice, which was studied by Goldstein [38] in some detail. The states of this random walk are those equidistant points at which the particle along its trajectory can hit either of the two planes confining the slit pore when it started with velocity \mathbf{v}_0 at $z_0 = -\frac{1}{2}\hat{L}$. Accordingly the distance between neighboring states is $d = v\tau$ and the time step is τ . After a collision with the wall, the particle proceeds moving in the direction into which it moved before the collision with probability p and changes its direction with probability $q = 1 - p$. The probabilities to arrive at the state kd from the left or from the right at time $t = n\tau$ are denoted by $\alpha(n, k)$ and $\beta(n, k)$, respectively. Under the assumption that the probabilities for a change of the direction are independent from each other in each particle wall collision, the probabilities $\alpha(n, k)$ and $\beta(n, k)$ satisfy the following discrete time Markovian master equations:

$$\begin{aligned} \alpha(n+1, k) &= p\alpha(n, k-1) + q\beta(n, k-1), \\ \beta(n+1, k) &= p\beta(n, k+1) + q\alpha(n, k+1), \end{aligned} \quad (11)$$

with the initial conditions

$$\alpha(1, k) = \delta_{k,1} \quad \text{and} \quad \beta(1, k) = 0, \quad (12)$$

which result from the assumption that the particle started with a positive velocity.

A formal solution of the persistent random walk is known in terms of the characteristic functions pertaining to the probabilities $\alpha(n, k)$ and $\beta(n, k)$ [38]. For our present purpose it is most important to note that the autocorrelation of the increments of the persistent random walk decays exponentially fast. Therefore the displacement of the particle is a sum of weakly correlated random numbers. The central limit theorem then applies and consequently the displacement becomes Gaussian distributed at long times t corresponding to large n .

Once the probabilities $\alpha(n, k)$ and $\beta(n, k)$ of the discrete time process are known, the probability density $\tilde{\rho}(\Delta x, t|\tau, v)$ can be determined as

$$\tilde{\rho}(\Delta x, t|\tau, v) = \sum_{n=0}^\infty f_n(\Delta x, t|\tau, v) I_n(t, \tau), \quad (13)$$

where $I_n(t, \tau)$ is the indicator function of the time interval between the n th and $(n+1)$ st particle collision with the wall, i.e.,

$$I_n(t, \tau) = \begin{cases} 1 & \text{if } n\tau \leq t < (n+1)\tau, \\ 0 & \text{otherwise,} \end{cases} \quad (14)$$

and where $f_n(\Delta x, t|\tau, v)$ specifying the probability density for this interval is given by

$$\begin{aligned} f_n(\Delta x, t|\tau, v) &= \sum_k \alpha(n+1, k+1) \delta(\Delta x - kd - v(t - n\tau)) \\ &\quad + \sum_k \beta(n+1, k-1) \delta(\Delta x - kd + v(t - n\tau)). \end{aligned} \quad (15)$$

Here the delta functions governing the deterministic motion of the particle between two collisions are weighted by the probabilities for the respective left and right running trajectories.

Using Eqs. (6) and (7) one can express the conditional second moment of the displacement $\langle \Delta \bar{x}^2(t) | \mathbf{v}_0 \rangle$ in terms of second moments $P_n(t, s)$ of the probability densities $f_n(\Delta x, t)$ and obtain for $n\tau \leq t < (n+1)\tau$

$$\langle \Delta \bar{x}^2(t) | \mathbf{v}_0 \rangle = \frac{1}{\tau} \int_0^{(n+1)\tau-t} P_n(t, s) ds + \frac{1}{\tau} \int_{(n+1)\tau-t}^\tau P_{n+1}(t, s) ds, \quad (16)$$

where

$$P_n(t, s) = \int_{-\infty}^\infty (x - vs)^2 f_n(x, t+s) dx. \quad (17)$$

By means of Eq. (15), $P_n(t, s)$ can be expressed by the total probabilities $\sum_k \alpha(n, k)$ and $\sum_k \beta(n, k)$ as well as by the first two moments of the individual probabilities $\alpha(n, k)$ and $\beta(n, k)$. It is convenient instead to consider linear combinations of the individual probabilities defined by

$$\begin{aligned} \gamma(n, k) &= \alpha(n, k) + \beta(n, k), \\ \eta(n, k) &= \alpha(n, k) - \beta(n, k). \end{aligned} \quad (18)$$

For the respective moments simple recursion relations can be derived which together with the initial conditions (12) lead to the following expressions:

$$\begin{aligned} \sum_k \gamma(n, k) &= 1, \\ \sum_k k \gamma(n, k) &= \frac{1}{2}(1+r)(1-c^n), \\ \sum_k k^2 \gamma(n, k) &= nr - \frac{1}{2}(r^2-1)(1-c^n), \end{aligned}$$

$$\sum_k \eta(n,k) = c^{n-1},$$

$$\sum_k k \eta(n,k) = \frac{1}{2}(1+r)(1-c^n), \quad (19)$$

where $r=p/q$ and $c=p-q$. The second moment $\sum k^2 \eta(n,k)$ vanishes exponentially fast for large values of n . With these results we find

$$\begin{aligned} P_n(t,s) = v^2 \tau^2 & \left[\frac{1}{2}(1-c^n)(2n+1-r^2) + n(n+rc^n) \right] \\ & + v^2 \tau [(1-c^n)(rt-2sn-t-2s) - 2nt] \\ & + 2v^2 s(1-c^n)(t+s) + v^2 t^2. \end{aligned} \quad (20)$$

By substituting Eq. (20) into Eq. (16), we obtain the explicit form of the conditional displacement $K(t|\tau, v)$ as follows:

$$K(t|\tau, v) = v^2 \left(a_n^{(1)} \tau^2 + a_n^{(2)} \tau + a_n^{(3)} t^2 + a_n^{(4)} \frac{t^3}{\tau} \right), \quad (21)$$

where $n\tau < t < (n+1)\tau$ ($n=0, 1, 2, \dots$) and

$$\begin{aligned} a_n^{(1)} &= n(1-c)c^n \left(\frac{1}{3}n^2 + \frac{1}{2}r^2 + r(n+1) \right) + (1-c^n) \left(\frac{1}{6} - \frac{1}{2}r^2 \right) \\ & - \frac{1}{2}nc^n(2nc+c+1), \\ a_n^{(2)} &= c^n[2cn - n(1-c)(2r+n) - r] + r, \\ a_n^{(3)} &= c^n[(1-c)(r+n) - c], \\ a_n^{(4)} &= -\frac{1}{3}c^n(1-c). \end{aligned} \quad (22)$$

Integrating $K(t|\tau, v)$ with respect to v_0^x and v_0^z [see Eq. (9)], we finally obtain $\langle \Delta \bar{x}^2(t) \rangle$. While the integration over v_0^x is straightforward, the integration over v_0^z does not lead to a closed form solution. We can obtain, however, an asymptotic expansion of $\langle \Delta \bar{x}^2(t) \rangle$ in the long time limit, which has the following form:

$$\langle \Delta \bar{x}^2(t) \rangle = At(B+C+2 \ln t) + O(1), \quad (23)$$

where

$$A = \sqrt{\frac{k_B T}{2\pi m}} \hat{L} r, \quad (24)$$

$$B = \begin{cases} 0 & \text{if } p = \frac{1}{2}, \\ \left(r - \frac{1}{3r} \right) [c + \ln c \operatorname{Ei}(1, -\ln c)] & \text{otherwise,} \end{cases}$$

(25)

$$C = \frac{6+c}{3r} - r - \gamma_{\text{EM}} + \ln \frac{2k_B T}{m \hat{L}^2}. \quad (26)$$

Here, $\gamma_{\text{EM}} = -\int_0^\infty e^{-x} \ln x dx$ is known as the Euler-Mascheroni constant and $\operatorname{Ei}(n, x) = \int_1^\infty t^{-n} e^{-xt} dt$ is the exponential integral. Note that the second moment of the displacement grows with $t \ln t$ slightly faster than it would do according to normal diffusion. By using the relation between the VACF and the MSD,

$$\langle \bar{\mathbf{v}}(t) \cdot \bar{\mathbf{v}}(0) \rangle = \frac{1}{2} \frac{d^2 \langle \Delta \bar{x}^2(t) \rangle}{dt^2}, \quad (27)$$

we obtain the following form of the long time behavior of the VACF:

$$\langle \bar{\mathbf{v}}(t) \cdot \bar{\mathbf{v}}(0) \rangle \approx At^{-1}. \quad (28)$$

It decays only as $1/t$. This is consistent with a diverging diffusion constant as discussed at the end Sec. III.

B. Analytical result for cylindrical pore system

Let us consider a cylindrical pore with radius R , whose axial direction is taken as the x axis. We choose the y axis such that the velocity \mathbf{v}_0 of the particle lies in the xy plane, i.e., $\mathbf{v}_0 = (v_0^x, v_0^y, 0)$ with $v_0^y \geq 0$. As in the case of the slit pore, we assume $v_0^x \geq 0$ without loss of generality. We assume that the initial position of the particle is at $(0, y_0, z_0)$ in the chosen coordinate system. Let $\hat{R} = R - \frac{1}{2}\sigma$ and $\Delta x = x(t) - x(0)$ denote the effective pore radius and the particle's displacement along the x axis, respectively. The behavior of the projected motion on the x axis, expressed by Δx , is governed by the same migration problem that was considered in the context of the slit pore problem. Just as in the case of the slit pore, we denote τ as the time between subsequent collisions, τ_0 as the time when the first collision occurs, and v as the constant speed of the projected motion. Then, these quantities are given in terms of the initial conditions as

$$\tau = \frac{2\sqrt{\hat{R}^2 - z_0^2}}{v_0^y}, \quad (29)$$

$$\tau_0 = \frac{\sqrt{\hat{R}^2 - z_0^2} - y_0}{v_0^y}, \quad (30)$$

$$v = v_0^x. \quad (31)$$

Therefore we can use the previous result in Eq. (21). However, in the case of the cylindrical pore, the time step τ is further dependent on the initial position, z_0 . So, if we want to know the ensemble-averaged MSD with respect to the initial position, we must perform an additional average over the distribution of z_0 ,

$$\langle \Delta x^2(t) | \mathbf{v}_0 \rangle = \int_{-\hat{R}}^{\hat{R}} K(t|\tau, v) \phi(z_0) dz_0. \quad (32)$$

For a uniform distribution of points with $y_0^2 + z_0^2 \leq \hat{R}^2$, one obtains

$$\phi(z_0) = \frac{2}{\pi \hat{R}^2} \sqrt{\hat{R}^2 - z_0^2} \quad \text{for } -\hat{R} \leq z_0 \leq \hat{R}. \quad (33)$$

By introducing a new variable,

$$\theta = \sin^{-1} \left(\frac{z_0}{\hat{R}} \right), \quad (34)$$

Eq. (32) becomes

$$\langle \Delta x^2(t) | \mathbf{v}_0 \rangle = \frac{2}{\pi} \int_{-\pi/2}^{\pi/2} K(t|\tau, v) \cos^2 \theta d\theta. \quad (35)$$

By taking the ensemble average with the initial velocity \mathbf{v}_0 , we have [compare with Eq. (9)]

$$\langle \Delta x^2(t) \rangle = \frac{2}{\pi} \int_{-\infty}^{\infty} dv_0^x \int_0^{\infty} dv_0^y \int_{-\pi/2}^{\pi/2} d\theta K(t|\tau, v) \psi(v_0^y, v_0^x) \cos^2 \theta. \quad (36)$$

From here, we can apply the same technique used in the case of the slit pore system. The asymptotic expansion of MSD and VACF in the long time limit can be written as follows:

$$\langle \Delta x^2(t) \rangle = \frac{16}{3} \sqrt{\frac{k_B T}{2\pi m}} \hat{R} t - \frac{1}{2} (3r^2 - 1) \hat{R}^2 \ln t + O(1), \quad (37)$$

$$\langle v_x(t) v_x(0) \rangle \approx \frac{1}{2} (3r^2 - 1) \hat{R}^2 t^{-2}. \quad (38)$$

This confirms that the dynamics of a rarified gas in a cylindrical pore follows the laws of normal diffusion.

III. COMPARISON WITH THE MOLECULAR DYNAMIC SIMULATION RESULTS

We consider two different geometrical shapes of nanopores confining N fluid particles—a slit pore with width L and a cylindrical pore with radius R . For the case of the slit pore, a rectangular structure of simulation cell with $V=L_x \times L_y \times L_z$ ($L_x=L_y \neq L_z, L_z=L$) is employed. Periodic boundary conditions are applied for the x and y directions, and two walls, parallel to each other and also to the xy plane, are located at $z = \pm \frac{1}{2}L$, respectively. For the case of the cylindrical pore, a cylindrical simulation cell with radius R and height L_x is employed with a periodic boundary condition at $x = \pm \frac{1}{2}L_x$. The fluid particle is considered as a hard sphere with diameter σ and mass m . The number density ρ is defined as N/V and the temperature T is obtained from the average kinetic energy obeying the equipartition theorem,

$$\frac{3}{2} N k_B T = \left\langle \frac{1}{2} \sum_{i=1}^N m \mathbf{v}_i^2 \right\rangle. \quad (39)$$

In our simulations, all physical quantities are given in dimensionless units by setting $k_B T$, m , and σ to unity. Accordingly, the time scale is also set as $\tau_{MD} = \sqrt{m \sigma^2 / k_B T} = 1$.

We performed molecular dynamics simulations for the systems consisting of 500 hard-sphere particles. Systems

with densities $\rho=0.0001$ and $\rho=0.01$ are studied, and the validity of the noninteracting particle assumption is checked. The desired number density is achieved, in the case of the slit pore, by adjusting the lengths along the x and y directions with fixed width $L=6$, and, in the case of the cylindrical pore, by adjusting the length L_x along the x direction with fixed radius $R=3$. We chose $L_x=L_y=912.87$ and $L_x=L_y=91.29$ for the slit pore, and $L_x=176\,838.83$ and $L_x=1768.39$ for the cylindrical pore to obtain the number density $\rho=0.0001$ and $\rho=0.01$, respectively.

The walls of both types of pores are smooth and hard. Three different simulations have been performed which are distinguished by the ways according to how particles are scattered at the walls. The first kind of wall considered is the MP wall, which has a simple enough structure to be employed for the analytical study. The particle, after scattered by this wall, reverses the transversal component of the moment, whereas its longitudinal component of the moment is either preserved or reversed according to a prescribed probability. The second one is the Knudsen wall, which scatters the fluid molecule in a fully random manner. Still it conserves the temperature of the fluid system by taking the velocity of the scattered particle from a Maxwell-Boltzmann distribution with specified temperature. In the third case of a Smoluchowski wall, the two types of particle wall collisions occur with an assigned probability: either the particle is scattered elastically, or after the collision it assumes a random velocity as in the case of a Knudsen wall.

Starting with the initial positions and velocities of the particles with uniform distribution and the Maxwell-Boltzmann distribution, respectively, the system is evolved via the discontinuous MD simulation method [39,40]. The trajectory of a given particle is determined by successive collision events. Since the particle performs a free motion between each collision, the equation of motion can be solved exactly up to the machine precision, which makes simulations stable over long periods of time.

The longitudinal MSDs computed from the MD simulations using the MP wall, the Knudsen wall, and the Smoluchowski wall were compared with the analytically obtained MSD [see Eqs. (23) and (37)]. The results are depicted in Fig. 1. In the asymptotic region ($\rho=0.0001$), the numerically obtained MSDs exactly match with the analytical results. This tells us that the noninteracting particle approximation is working well in this density regime. From the simulations, it is also revealed that the MSDs obtained by using the MP wall show the same behavior as those obtained for the Knudsen-Smoluchowski wall when the fraction of thermal scattering α [see Eq. (41)] and the reversal probability q of the MP wall satisfy the relation $\alpha=2q$.

The action of a given wall on a colliding particle can be characterized by a transfer function relating the incoming particle velocity \mathbf{u} to the outgoing velocity \mathbf{v} . In the cases of the MP and the Knudsen-Smoluchowski walls, the relevant part of the transfer function is given by the probability density for the parallel component of the velocity v after a collision on the condition that the parallel component of the incoming velocity is assigned as u . For the MP wall v equals u with probability $1-q$ and $-u$ with probability q , respectively. For the Smoluchowski wall the collision is elastic, i.e.,

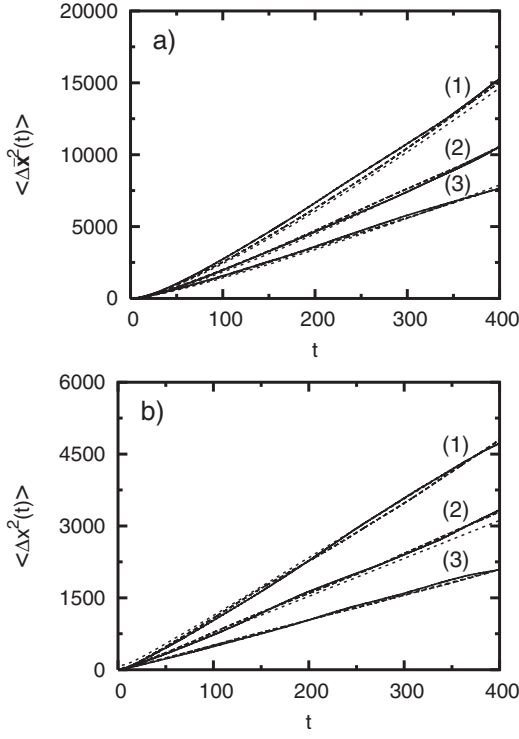


FIG. 1. Plots of MSD as a function of time obtained from the MD simulations for various values of q and α (a) for the slit pore system and (b) for the cylindrical pore system at $\rho=0.0001$. The MSD using the MP wall is plotted with solid lines and the MSD using the Knudsen-Smoluchowski wall is plotted with dashed lines. The analytical results of MSD are displayed with dotted lines. (1) $q=0.3$, $\alpha=0.6$; (2) $q=0.4$, $\alpha=0.8$; and (3) $q=0.5$, $\alpha=1$.

$v=u$ with probability $1-\alpha$ and, with probability α , takes a random value out of the Maxwell-Boltzmann distribution $f(v)=\sqrt{\frac{m}{2\pi k_B T}} \exp(-\frac{mv^2}{2k_B T})$. Consequently the transfer functions of the two walls become

$$g^{\text{MP}}(v|u) = (1-q)\delta(v-u) + q\delta(v+u), \quad (40)$$

$$g^{\text{Smoluchowski}}(v|u) = (1-\alpha)\delta(v-u) + \alpha f(v). \quad (41)$$

One confirms by inspection that both transfer functions leave the Maxwell-Boltzmann distribution invariant, i.e.,

$$\int_{-\infty}^{\infty} g(v|u)f(u)du = f(v). \quad (42)$$

In order to further examine the properties of the two walls, we calculate each n th moment $\langle v^n|u \rangle$ associated with the transfer functions defined in Eqs. (40) and (41), respectively. For the MP wall described by Eq. (40), the n th moment becomes

$$\langle v^n|u \rangle = \begin{cases} u^{2k}, & n=2k \\ (1-2q)u^{2k+1}, & n=2k+1, \end{cases} \quad (43)$$

and for the Smoluchowski wall described by Eq. (41)

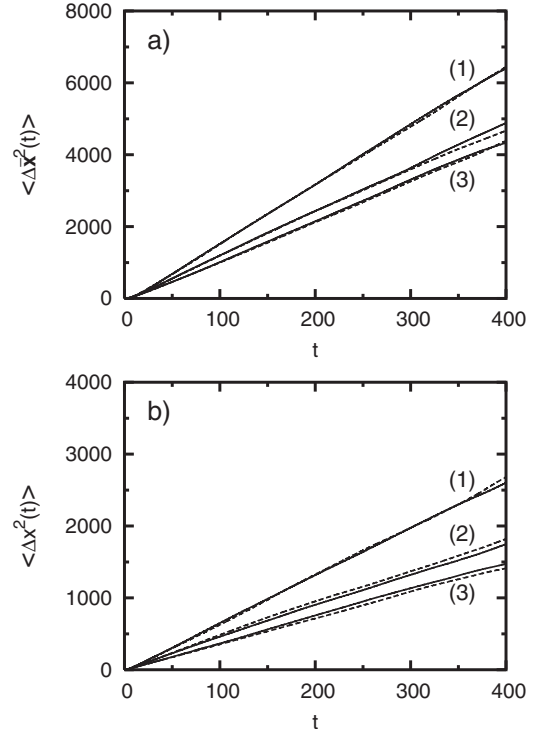


FIG. 2. Plots of MSD as a function of time obtained from the MD simulations for various values of q and α (a) for the slit pore system and (b) for the cylindrical pore system at $\rho=0.01$. The MSD using the MP wall is plotted with solid lines and the MSD using the Knudsen-Smoluchowski wall is plotted with dashed lines. (1) $q=0.3$, $\alpha=0.6$; (2) $q=0.4$, $\alpha=0.8$; and (3) $q=0.5$, $\alpha=1$.

$$\langle v^n|u \rangle = \begin{cases} u^{2k} - \alpha(u^{2k} - \langle u^{2k} \rangle), & n=2k \\ (1-\alpha)u^{2k+1}, & n=2k+1, \end{cases} \quad (44)$$

where

$$\langle u^{2k} \rangle = \int u^{2k} f(u) du = \frac{(2k)!}{2^k k!} \left(\frac{k_B T}{m} \right)^k. \quad (45)$$

The comparison of Eq. (43) with Eq. (44) reveals that the condition, $\alpha=2q$, makes all odd order moments associated with the two transfer functions identical to each other. The even moments differ by $\alpha(u_i^{2k} - \langle u_i^{2k} \rangle)$. However, this term vanishes if we take the equilibrium ensemble average with respect to the velocity u before the collision. Thus, when $\alpha=2q$, the moments of equal order n associated with the two transfer functions coincide with each other in equilibrium state. Figure 2 reveals that the coincidence between the MSD obtained using the MP wall and that obtained using the Smoluchowski wall holds not only in the low density regime ($\rho=0.0001$) but also for the much higher density $\rho=0.01$.

The self-diffusion coefficients along the longitudinal direction are defined as

$$D^{\text{slit}} = \lim_{t \rightarrow \infty} \frac{\langle \Delta \bar{x}^2(t) \rangle}{4t} \quad (46)$$

for the slit pore and

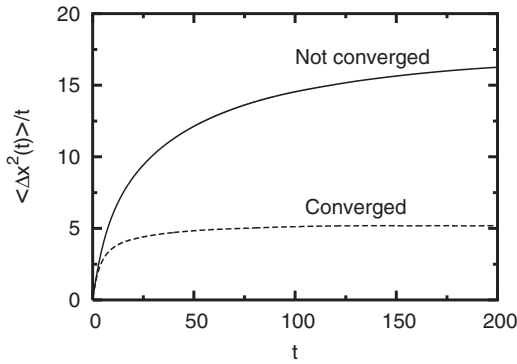


FIG. 3. Plots of $\langle \Delta x^2(t) \rangle / t$ as a function of time obtained from the MD simulations with the Knudsen wall at $\rho=0.0001$. The MSD for the slit pore system is shown with a solid line and the MSD for the cylindrical pore system is shown with a dashed line.

$$D^{\text{cylinder}} = \lim_{t \rightarrow \infty} \frac{\langle \Delta x^2(t) \rangle}{2t} \quad (47)$$

for the cylindrical pore, respectively. Therefore from Eqs. (23) and (37), the analytically obtained self-diffusion coefficients for the slit and cylindrical pore are

$$D^{\text{slit}} = \lim_{t \rightarrow \infty} \frac{A}{2} (B + C + 2 \ln t), \quad (48)$$

$$D^{\text{cylinder}} = \frac{8}{3} \sqrt{\frac{k_B T}{2\pi m}} \hat{R} r, \quad (49)$$

respectively, where A , B , and C are defined in Eqs. (24)–(26). The diffusion coefficient for the slit pore, D^{slit} , shows a logarithmic divergence as a function of time in the long time region, whereas the diffusion coefficient D^{cylinder} of the cylindrical pore is constant with respect to time [18,27]. These different kinds of behavior are confirmed by the simulation results for $\langle \Delta x^2(t) \rangle / t$ as a function of t using the Knudsen wall model ($\alpha=1$) at the density ($\rho=0.0001$) (see Fig. 3). As time increases, $\langle \Delta x^2(t) \rangle / t$ of the cylindrical pore system shows fast convergence to a finite value. However, no convergence is obtained for the respective quantity $\langle \Delta x^2(t) \rangle / t$ in the case of the slit pore.

This divergence of the self-diffusion coefficient in the slit pore system can also be inferred from the behavior of the VACF. The Green-Kubo relation tells us that the self-diffusion coefficient is related with the VACF as [39]

$$D_x = \lim_{t \rightarrow \infty} \int_0^t \langle v_x(t) v_x(0) \rangle dt. \quad (50)$$

If the VACF decays faster than t^{-1} , then Eq. (50) yields a finite self-diffusion coefficient. If it decays as t^{-1} , the right-hand side of Eq. (50) diverges logarithmically. According to our analytical results as shown in Eqs. (28) and (38), the VACF of the slit pore behaves as t^{-1} , and the VACF of the cylindrical pore decays as t^{-2} . The log-log plots of VACF versus time obtained from the MD simulations using the Knudsen wall model are depicted in Fig. 4 for $\rho=0.0001$.

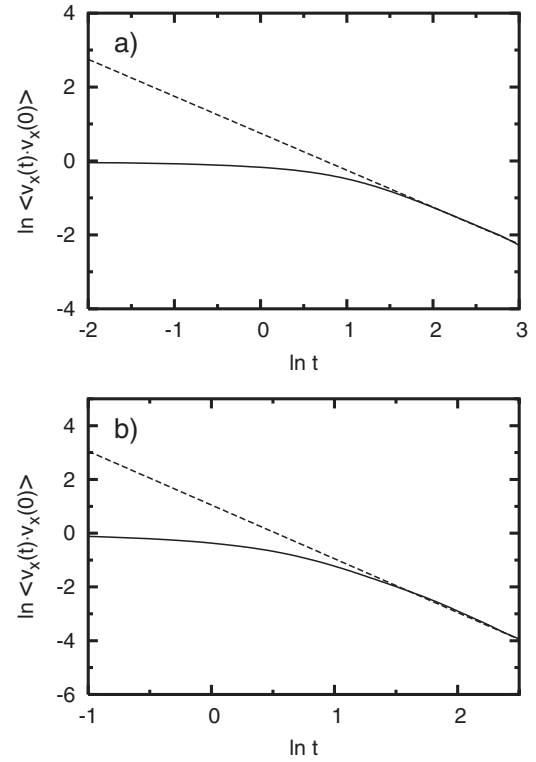


FIG. 4. Log-log plots of VACF obtained from the MD simulations as functions of time (a) for the slit pore system and (b) for the cylindrical pore system at $\rho=0.0001$ with Knudsen wall model (solid lines). The dashed lines having slopes (a) -1 and (b) -2 , respectively, are displayed to facilitate the comparison.

Both cases show algebraic decaying patterns in the long time limit, and the slopes obtained from the plots well match with the analytical results.

IV. CONCLUSIONS

Wall-mediated transport phenomena in micropores with two prototypes of geometries were investigated by both analytical and numerical means. The MP wall, due to its simplicity, provides a complete analytical description of the self-diffusion behavior of simple fluids for both slit and cylindrical pores in the regime of large Knudsen numbers. The diffusion process through the cylindrical pore obeys Fick's law, as it is well-known from previous studies. On the other hand, the diffusion coefficient in slit pores obtained from the time dependence of the MSD and the VACF consistently shows a logarithmic divergence. Our molecular dynamic simulation results confirmed these analytical predictions. We further showed that two different types of thermal walls, the MP wall and the Knudsen wall/Smoluchowski wall are equivalent for a proper choice of the reversal probability; not only in the low density region but also in the intermediate density region where the relative magnitude of the collision rate between particles is comparable to the wall-particle collision rate. Finally we note that a modification of the details of the particle-wall interaction will not change the dynamics at large times as long as the Maxwell boundary conditions hold.

ACKNOWLEDGMENTS

This work was supported by the Korea Research Foundation funded by the Korean Government (MOEHRD, Basic Research Promotion Fund) Grant No. KRF-2005-070-C00065, by the Korea Science and Engineering Foundation

Grant No. F01-2006-000-10194-0, by the German Excellence Initiative via *Nanosystems Initiative Munich (NIM)*, by the KOMSCO, and by the Deutsche Forschungsgemeinschaft and the Korea Science and Engineering Foundation in the framework of the joint KOSEF-DFG Contract No. 446 KOR 113/21/01-1.

-
- [1] F. Gambale, M. Bregante, F. Stragapede, and A. M. Cantu, *J. Membr. Biol.* **154**, 69 (1996).
- [2] Z. Siwy, I. D. Kosińska, A. Fuliński, and C. R. Martin, *Phys. Rev. Lett.* **94**, 048102 (2005).
- [3] D. Reguera, G. Schmid, P. S. Burada, J. M. Rubi, P. Reimann, and P. Hänggi, *Phys. Rev. Lett.* **96**, 130603 (2006).
- [4] B. J. Hinds, N. Chopra, T. Rantell, R. Andrews, V. Gavalas, and L. G. Bachas, *Science* **303**, 62 (2004).
- [5] C. T. Kresge, M. E. Leonowicz, W. J. Roth, J. C. Vartuli, and J. S. Beck, *Nature (London)* **359**, 710 (1992).
- [6] M. E. Davis, *Nature (London)* **417**, 813 (2002).
- [7] A. Katz and M. E. Davis, *Nature (London)* **403**, 286 (2000).
- [8] K. Hahn, J. Kärger, and V. Kukla, *Phys. Rev. Lett.* **76**, 2762 (1996).
- [9] V. Gupta, S. S. Nivarthi, D. Keffer, A. V. McCormick, and H. T. Davis, *Science* **274**, 164 (1996).
- [10] B. C. H. Steele and A. Heinzl, *Nature (London)* **274**, 164 (1996).
- [11] O. G. Jepps, S. K. Bhatia, and D. J. Searles, *Phys. Rev. Lett.* **91**, 126102 (2003).
- [12] S. K. Bhatia and D. Nicholson, *Phys. Rev. Lett.* **90**, 016105 (2003).
- [13] S. K. Bhatia and D. Nicholson, *J. Chem. Phys.* **119**, 1719 (2003).
- [14] O. G. Jepps, S. K. Bhatia, and D. J. Searles, *J. Chem. Phys.* **120**, 5396 (2004).
- [15] S. K. Bhatia, O. G. Jepps, and D. Nicholson, *J. Chem. Phys.* **120**, 4472 (2004).
- [16] S. K. Bhatia and D. Nicholson, *AIChE J.* **52**, 29 (2006).
- [17] G. Arya, H.-C. Chang, and E. J. Maginn, *J. Chem. Phys.* **115**, 8112 (2001).
- [18] G. Arya, H.-C. Chang, and E. J. Maginn, *Phys. Rev. Lett.* **91**, 026102 (2003).
- [19] G. Arya, H.-C. Chang, and E. J. Maginn, *Mol. Simul.* **29**, 697 (2003).
- [20] K. Hahn and J. Kärger, *J. Phys. Chem.* **100**, 316 (1996).
- [21] L. A. Pozhar and K. E. Gubbins, *J. Chem. Phys.* **99**, 8970 (1993).
- [22] L. A. Pozhar and K. E. Gubbins, *Int. J. Thermophys.* **20**, 805 (1999).
- [23] K. P. Travis and K. E. Gubbins, *J. Chem. Phys.* **112**, 1984 (2000).
- [24] K. P. Travis and K. E. Gubbins, *Mol. Simul.* **25**, 209 (2000).
- [25] V. P. Sokhan, D. Nicholson, and N. Quirke, *J. Chem. Phys.* **115**, 3878 (2001).
- [26] V. P. Sokhan, D. Nicholson, and N. Quirke, *J. Chem. Phys.* **117**, 8531 (2002).
- [27] M. Knudsen, *Ann. Phys.* **333**, 75 (1909).
- [28] W. G. Pollard and R. D. Present, *Phys. Rev.* **73**, 762 (1948).
- [29] H. T. Davis, in *Fundamentals of Inhomogeneous Fluids*, edited by D. Hendersen (Dekker, New York, 1992).
- [30] C. Rhykerd, Z. Tan, L. A. Pozhar, and K. E. Gubbins, *J. Chem. Soc., Faraday Trans.* **87**, 2011 (1991).
- [31] I. Bitsanis, T. K. Vanderlick, M. Tirrell, and H. T. Davis, *J. Chem. Phys.* **89**, 3152 (1988).
- [32] M. v. Smoluchowski, *Ann. Phys.* **338**, 1559 (1910).
- [33] R. Tehver, F. Toigo, J. Koplik, and J. R. Banavar, *Phys. Rev. E* **57**, R17 (1998).
- [34] A. Tenenbaum, G. Ciccotti, and R. Gallico, *Phys. Rev. A* **25**, 2778 (1982).
- [35] J. C. Maxwell, *Philos. Trans. R. Soc. London* **170**, 231 (1879).
- [36] K. K. Mon and J. K. Percus, *J. Chem. Phys.* **119**, 3343 (2003).
- [37] K. K. Mon, J. K. Percus, and J. Yan, *Mol. Simul.* **29**, 721 (2003).
- [38] S. Goldstein, *Q. J. Mech. Appl. Math.* **4**, 1951 (1950).
- [39] M. P. Allen and D. J. Tildesley, *Computer Simulation of Liquids* (Clarendon, Oxford, 1987).
- [40] R. Chang, K. Jagannathan, and A. Yethiraj, *Phys. Rev. E* **69**, 051101 (2004).